veterinary sciences

MDPI

Article

m6A Methylation and Transcriptomic Responses in the Bovine Mammary Gland Following Intramammary *Escherichia coli* Challenge

Yanru Wang [1,2], Huimin Zhang [1,2], Mingxun Li [1,2], Niel A. Karrow [3] and Yongjiang Mao [1,2,*]

[1] Key Laboratory for Animal Genetics, Breeding, Reproduction and Molecular Design of Jiangsu Province, College of Animal Science and Technology, Yangzhou University, Yangzhou 225009, China; dx120210150@stu.yzu.edu.cn (Y.W.); minmin-911@163.com (H.Z.); limingxun@live.com (M.L.)
[2] Joint International Research Laboratory of Agriculture and Agri-Product Safety, Yangzhou University, Yangzhou 225009, China
[3] Center for Genetic Improvement of Livestock, Department of Animal Biosciences, University of Guelph, Guelph, ON N1G2W1, Canada; nkarrow2@gmail.com
* Correspondence: cattle@yzu.edu.cn

Simple Summary

Bovine mastitis caused by *Escherichia coli* is characterized by a rapid inflammatory response in the mammary gland. RNA m6A methylation is known to participate in gene regulation, but its involvement in bovine mastitis is not well defined. Here, we examined mammary tissues collected after different durations of *E. coli* exposure and combined m6A profiling with transcriptome analysis. The two exposure groups showed clear differences in both RNA methylation and gene-expression patterns, particularly in pathways related to inflammation and immunity. These results provide candidate genes and biological processes for further investigation of m6A-associated regulation in bovine mastitis.

Abstract

Escherichia coli is an important cause of bovine mastitis and induces inflammatory responses in the mammary gland. N6-methyladenosine (m6A) is an important post-transcriptional RNA modification involved in gene regulation, but its association with the bovine mammary response to *E. coli* remains unclear. In this study, a within-cow mammary-quarter design was used in four clinically healthy Holstein cows, with quarters assigned to saline control, 12 h *E. coli* exposure, and 24 h *E. coli* exposure groups. MeRIP-seq and RNA-seq were integrated to characterize m6A enrichment and gene expression, with cow identity accounted for in the differential analyses. Compared with the saline control, 2242 and 1848 differential m6A peaks were identified in the 12 h and 24 h exposure groups, respectively. RNA-seq identified 591 differentially expressed genes (DEGs) in the 12 h exposure group and 1287 DEGs in the 24 h exposure group. Integrated analysis identified 264 and 476 differentially m6A peak-gene associations in the 12 h and 24 h exposure groups, respectively. Functional enrichment analysis showed that differential m6A peak-gene associations were mainly involved in immune and inflammatory processes, including NF-κB, NOD-like receptor, IL-17, and TNF signaling pathways. The patterns of m6A enrichment and gene expression differed between the exposure groups, although these differences cannot be attributed to exposure duration alone because of the staggered inoculation design. These findings indicate that changes in m6A enrichment are associated with gene expression during the bovine mammary response to *E. coli* challenge and provide candidate genes for further investigation of m6A-related regulation in bovine mastitis.

Check for updates

Academic Editor: Jinhu Huang

Received: 23 September 2026
Revised: 29 October 2026
Accepted: 30 October 2026
Published: 4 November 2026

Copyright: © 2026 by the authors. Licensee MDPI, Basel, Switzerland. This article is an open access article distributed under the terms and conditions of the Creative Commons Attribution (CC BY) license.

Keywords: Bovine mastitis; m6A methylation; *Escherichia coli*; MeRIP-seq; RNA-seq; immune response

1. Introduction

N6-methyladenosine (m6A), first identified in the 1970s, is a widespread post-transcriptional modification of messenger RNA, non-coding RNA, and viral RNA [1]. Its deposition, removal, and recognition are mediated by writer proteins such as the METTL3-METTL14 complex [2], erasers such as FTO and ALKBH5 [3], and readers such as YTH-domain proteins [4]. Through effects on RNA splicing, stability, translation, and degradation, m6A contributes to embryonic development, metabolic homeostasis, and immune regulation [5,6]. m6A modification is involved in a wide range of biological processes and has been implicated in the regulation of nervous system function and liver biology and metabolism [7,8]. Altered m6A regulation has also been reported in inflammatory and immune-mediated diseases [9,10].

Mastitis is among the most common and costly diseases of dairy cattle. It compromises animal welfare, milk yield, and milk quality and imposes substantial costs on dairy production [11]. Milking practices can also influence susceptibility to intramammary infection by affecting teat tissue integrity, microbial exposure, and the maintenance of teat canal defenses [12]. Escherichia coli is a major environmental cause of clinical and subclinical bovine mastitis [13]. Clinical infection may produce udder swelling and pain, abnormal milk, fever, anorexia, reduced milk yield, and, in severe cases, death [14–16]. Subclinical infection is commonly associated with increased milk somatic cell counts and altered inflammatory mediator concentrations [17,18]. Some *E. coli* strains also present a food-safety concern when contaminated raw milk or dairy products enter the food chain [19].

Escherichia coli can induce a rapid inflammatory response in the mammary gland. Following recognition of bacterial components by mammary epithelial cells and resident immune cells, inflammatory signaling promotes cytokine production and leukocyte recruitment to the site of infection [20]. Lipopolysaccharide (LPS), a major component of the Gram-negative bacterial outer membrane, is an important trigger of this response [21–24]. Although the inflammatory response is essential for bacterial clearance, excessive or prolonged activation can contribute to mammary tissue damage. Previous transcriptomic studies have revealed extensive changes in immune- and inflammation-related gene expression following intramammary *E. coli* challenge, providing important insights into the transcriptional response of the bovine mammary gland. However, it remains unclear how m6A enrichment changes in bovine mammary tissue following *E. coli* challenge and whether these changes are associated with the accompanying transcriptional response.

The bovine udder contains four anatomically separate mammary quarters, allowing quarters within the same cow to serve as experimental units in intramammary challenge studies [25]. Quarter-level health status and inflammatory stimulation can affect milk composition [26,27], while persistent inflammation can damage mammary lobules and ducts and impair lactation [28]. Based on this anatomical organization, a within-cow mammary-quarter design was used in the present study. We combined MeRIP-seq and RNA-seq to characterize m6A methylation and transcriptomic profiles in saline-treated control quarters and quarters exposed to *E. coli* for 12 or 24 h. By integrating differential m6A methylation with gene expression profiles, we aimed to identify candidate genes and biological processes associated with the bovine mammary response to *E. coli* challenge.

2. Materials and Methods

2.1. Experimental Animal Selection and Management

Four clinically healthy, second-parity Holstein cows, each 4 years old and at 130–180 days in milk (DIM), were selected from a dairy farm in Xuzhou, Jiangsu Province, China. Daily milk yield on the day before challenge ranged from 17.2 to 22.9 kg/cow/day. The farm maintained individual health records for all cows, which were reviewed for the 2 months preceding the experiment. Quarter milk samples were collected separately, and only mammary quarters with SCC <200,000 cells/mL were included in the experiment. Beginning 1 week before challenge, milk somatic cell count (SCC) was measured daily to further assess mammary health. Somatic cell score (SCS) was calculated from somatic cell count (SCC) according to the following transformation:

$$SCS = \log_2(SCC/100{,}000) + 3$$

Rectal temperature was measured at −24, −12, 0, 6, 12, and 24 h relative to the initial *Escherichia coli* inoculation to monitor the clinical response. Cows were housed individually under standardized management conditions.

2.2. Escherichia coli Preparation and Intramammary Inoculation

Escherichia coli ATCC 25922 (CGMCC 1.2385) was obtained from the China General Microbiological Culture Collection Center (CGMCC, Beijing, China). ATCC 25922 was selected as a well-characterized reference strain to provide a standardized and reproducible bacterial challenge. A similar intramammary challenge model using *E. coli* ATCC 25922 has previously been established in dairy cows [29]. The lyophilized strain was rehydrated and streaked onto solid medium. The viable bacterial concentration was determined by serial dilution, plating, incubation, and colony counting. The bacterial suspension was adjusted to 1×10^5 CFU/mL based on the colony counts. Each challenged mammary quarter received 5 mL of the bacterial suspension, corresponding to a total inoculum of 5×10^5 CFU per quarter. Before inoculation, residual milk was completely removed from the designated mammary quarters. The udder surface was rinsed with warm water and disinfected three times with cotton balls soaked in 75% ethanol. Subsequent procedures were performed after the ethanol had evaporated. Five milliliters of the *E. coli* suspension (1×10^5 CFU/mL) was administered through the teat canal using a needle-free syringe. Following inoculation, the udder was gently massaged for 10 min to facilitate distribution of the bacterial suspension within the mammary gland.

2.3. Experimental Design and Sample Collection

A within-animal mammary-quarter design was used. The four mammary quarters of each cow were assigned to a 24 h *E. coli* challenge, a 12 h *E. coli* challenge, a sterile saline control, and an untreated control (Figure 1). Treatment positions were balanced across cows such that each treatment occurred once at each mammary-quarter position. No formal randomization procedure was used. At 0 h, one quarter was inoculated with *E. coli* and another received sterile saline; at 12 h, a third quarter was inoculated with *E. coli*, while the remaining quarter was left untreated. Mammary tissues from all four quarters were collected at the common 24 h endpoint. Thus, quarters inoculated at 0 and 12 h represented the 24 h and 12 h exposure groups, respectively. The saline-treated quarters were used as the sequencing control because they underwent the same intramammary administration procedure as the challenged quarters but without bacterial exposure. The untreated quarters served as an additional reference for baseline mammary status but were not included in the sequencing analysis.

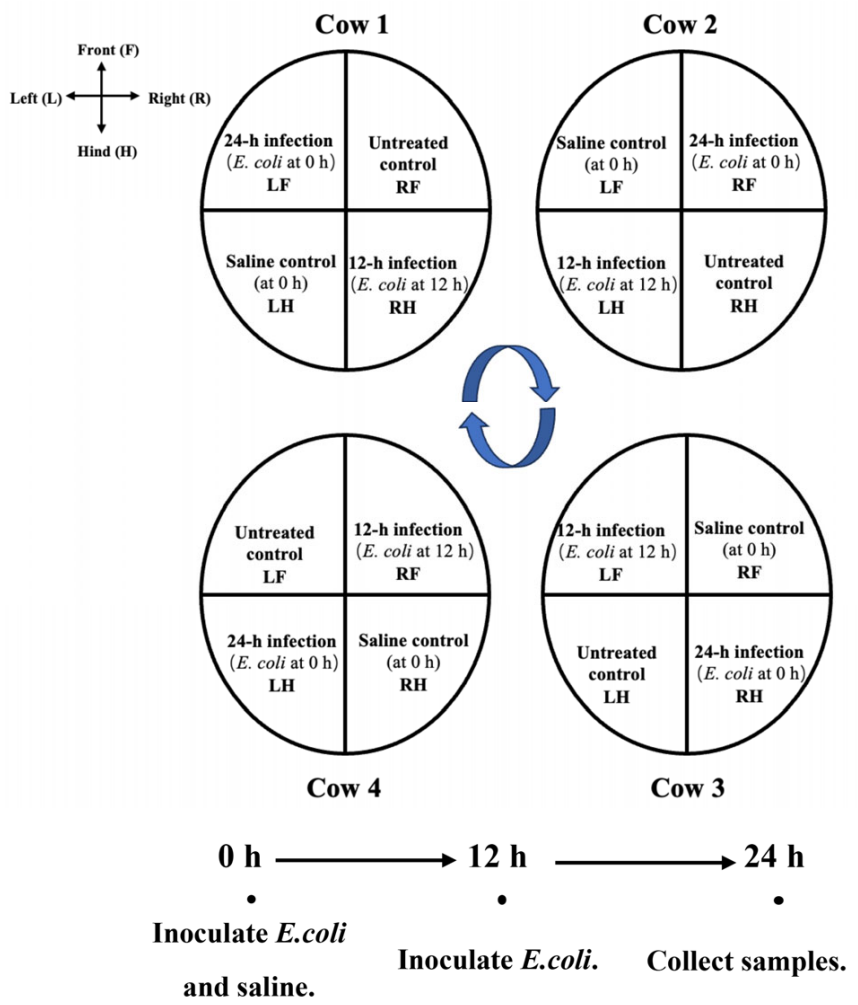


Figure 1. Experimental design and mammary-quarter treatment allocation. LF, left fore quarter; RF, right fore quarter; LH, left hind quarter; RH, right hind quarter.

Mammary tissue samples were collected from a region adjacent to the teat at the common 24 h experimental endpoint. After incision through the skin, subcutaneous tissue, and mammary gland capsule, approximately 1 g of mammary parenchymal tissue was collected from each quarter. Approximately 2 h before mammary tissue collection, the cows were sedated with xylazine (20 μg/kg, intravenously). Before biopsy, 3 mL of lidocaine hydrochloride was infiltrated locally above the biopsy site to provide local anesthesia. Tissue samples for molecular analyses were immediately frozen in liquid nitrogen, whereas samples for histological examination were immediately placed in fixative. Yunnan Baiyao was applied for hemostasis after tissue collection, and the cows received intravenous antibiotic treatment once daily for 1 week.

2.4. RNA Extraction and MeRIP-Seq

Total RNA was extracted from mammary tissue using TRIzol reagent (Invitrogen, Carlsbad, CA, USA). RNA concentration and purity were measured using a NanoDrop ND-1000 (NanoDrop Technologies, Wilmington, DE, USA), and RNA integrity was assessed using an Agilent 2100 Bioanalyzer (Agilent Technologies, Santa Clara, CA, USA). Samples with RIN > 7.0, OD260/280 > 1.8, RNA concentration > 50 ng/μL, and total RNA > 1 μg were used for library preparation. Total RNA was fragmented at 94 °C for 5 min using the NEBNext Magnesium RNA Fragmentation Module (New England Biolabs, Ipswich, MA, USA; Cat. No. E6150S). Fragmented RNA from each biological sample was divided into

matched IP and input fractions. For m6A immunoprecipitation, an m6A-specific antibody (Synaptic Systems GmbH, Göttingen, Germany; Cat. No. 202003) coupled to Dynabeads using the Dynabeads Antibody Coupling Kit (Invitrogen, Carlsbad, CA, USA) was used to enrich m6A-containing RNA fragments. The matched input fraction was retained without immunoprecipitation and processed in parallel for library preparation. Libraries generated from the matched IP and input fractions were sequenced on an Illumina NovaSeq 6000 platform (Illumina, Inc., San Diego, CA, USA) using 150-bp paired-end sequencing.

2.5. Bioinformatics Analysis

Raw reads were quality filtered using fastp (v0.19.4) and aligned to the Bos taurus reference genome ARS-UCD2.0 (RefSeq accession: GCF_002263795.3) using HISAT2 (v2.2.1), allowing up to 20 alignments per read and a maximum of two mismatches. For MeRIP-seq analysis, m6A peaks and differential m6A peaks were identified using the exomePeak R/Bioconductor package. Peak annotation was performed using ANNOVAR (https://annovar.openbioinformatics.org), and motif analysis was conducted using HOMER (v4.1) with the parameters -size 200 and -len 5, 8, 10. For RNA-seq analysis, gene expression was quantified using StringTie (v2.1.2), and DEGs were identified using DESeq2. For both RNA-seq and MeRIP-seq differential analyses, cow identity was included as a blocking factor to account for the paired within-cow experimental design. For MeRIP-seq, IP enrichment was evaluated relative to the corresponding input from the same biological sample. Differential m6A peaks and DEGs with $|\log2FC| \geq 1$ and FDR <0.05 were considered significant. For the integrated analysis, differential m6A peaks were assigned to genes according to their genomic annotation and intersected with the corresponding DEG lists. Each differential peak–gene pair was retained as an individual association. Thus, genes associated with multiple differential m6A peaks could contribute more than one association, and peaks with opposite directions of m6A enrichment were classified separately according to their respective log2FC values. Associations were categorized as Hyper-Up, Hyper-Down, Hypo-Up, or Hypo-Down according to the direction of differential m6A enrichment and gene expression.

For peak-associated functional enrichment analyses, genes associated with multiple differential m6A peaks were counted once. GO and KEGG enrichment analyses were performed using a hypergeometric test against the genome-wide annotated gene background. p values were adjusted for multiple testing, and terms or pathways with FDR < 0.05 were considered significantly enriched. The top significantly enriched GO terms or KEGG pathways ranked by FDR were selected for visualization.

2.6. Quantitative Real-Time Polymerase Chain Reaction (RT-qPCR)

Total RNA was reverse-transcribed into cDNA using HiScript Reverse Transcriptase (Vazyme Biotech Co., Ltd., Nanjing, China). Based on the mRNA sequences of the target genes and the bovine reference gene GAPDH retrieved from the NCBI database, RT-qPCR primers were designed using Primer Premier 6 software. RT-qPCR was performed using SupRealQ Ultra SYBR qPCR Master Mix (Vazyme Biotech Co., Ltd., Nanjing, China) on an Applied Biosystems QuantStudio 3 Real-Time PCR System (Thermo Fisher Scientific, Waltham, MA, USA). All primers were synthesized by Tsingke Biotechnology Co., Ltd. (Beijing, China). Each biological sample was analyzed in 3 technical replicates. GAPDH was used as the reference gene. GAPDH Ct values showed limited variation across the experimental conditions, supporting its use as an internal reference. Relative gene expression was calculated using the $2^{-\Delta\Delta Ct}$ method. Detailed information of the primers is listed in Table 1.

Table 1. Primer sequences.

Gene	NCBI Accession No.	Primer Sequence (5′–3′)	Product Size (bp)
IL6	NM_173923.2	F: ATCCTGAAGCAAAAGATCGCAG R: AATCATGGGAGCCCCAGCTA	188
CXCL8	NM_173925.2	F: AACGAGGTCTGCCTAAACCC R: TCTTGCTTCTCAGCTCTCTTCA	80
TNF-α	NM_173966.3	F: ATTAGGGATGTAGGGAAGTGAGG R: CAAGGAATGTTGCGAAGTGTT	175
GAPDH	NM_001034034.2	F: AAGGTCGGAGTGAACGGATTC R: ATGGCGACGATGTCCACTTT	86

2.7. Histopathological Examination

Mammary tissue samples were fixed, sectioned, and stained with hematoxylin and eosin (H&E) by Wuhan Servicebio Technology Co., Ltd. (Wuhan, China). Histopathological changes in mammary tissue were subsequently examined by light microscopy.

2.8. Statistical Analysis

Statistical analyses were performed using GraphPad Prism version 10.5.0 (673) (GraphPad Software, Boston, MA, USA). Data are presented as mean ± SEM. SCS was calculated as SCS = $\log_2$(SCC/100,000) + 3. SCS in untreated and saline-treated quarters was analyzed using two-way repeated-measures ANOVA followed by Šídák's multiple-comparisons test. SCS in the 12 h *E. coli* group was analyzed using a paired *t*-test, whereas SCS in the 24 h *E. coli* group and rectal temperature were analyzed using one-way repeated-measures ANOVA followed by Dunnett's multiple-comparisons test, with 0 h as the reference. Cow identity was used as the matching factor in the repeated-measures analyses. RT-qPCR relative expression values calculated using the $2^{-\Delta\Delta Ct}$ method were analyzed using one-way repeated-measures ANOVA followed by Dunnett's multiple-comparisons test, with cow identity used as the matching factor. Differences were considered significant at $p < 0.05$.

3. Results

3.1. Establishment of an Escherichia coli-Induced Bovine Mastitis Model

No significant differences in SCS were observed between the untreated and saline-treated quarters at 0, 12, or 24 h (Figure 2A). In the E. coli_12 group, SCS increased significantly at 12 h after inoculation compared with the pre-inoculation level ($p < 0.001$). In the E. coli_24 group, SCS was also significantly increased at 12 and 24 h after inoculation ($p < 0.01$ and $p < 0.05$, respectively).

Rectal temperature increased following *E. coli* challenge, with significant increases observed at 6, 12, and 24 h compared with 0 h (Figure 2B). Histological examination showed relatively intact mammary tissue structure in the untreated and saline groups, whereas inflammatory cell infiltration and tissue structural alterations were observed following *E. coli* challenge (Figure 2C). These histopathological changes were evident in both the E. coli_12 and E. coli_24 groups.

RT-qPCR analysis further showed that the mRNA expression levels of *IL-6*, *CXCL8*, and *TNF-α* were significantly increased following *E. coli* challenge compared with the saline group (Figure 2D). Collectively, these results confirmed that intramammary *E. coli* challenge induced a clear inflammatory response in the mammary gland.

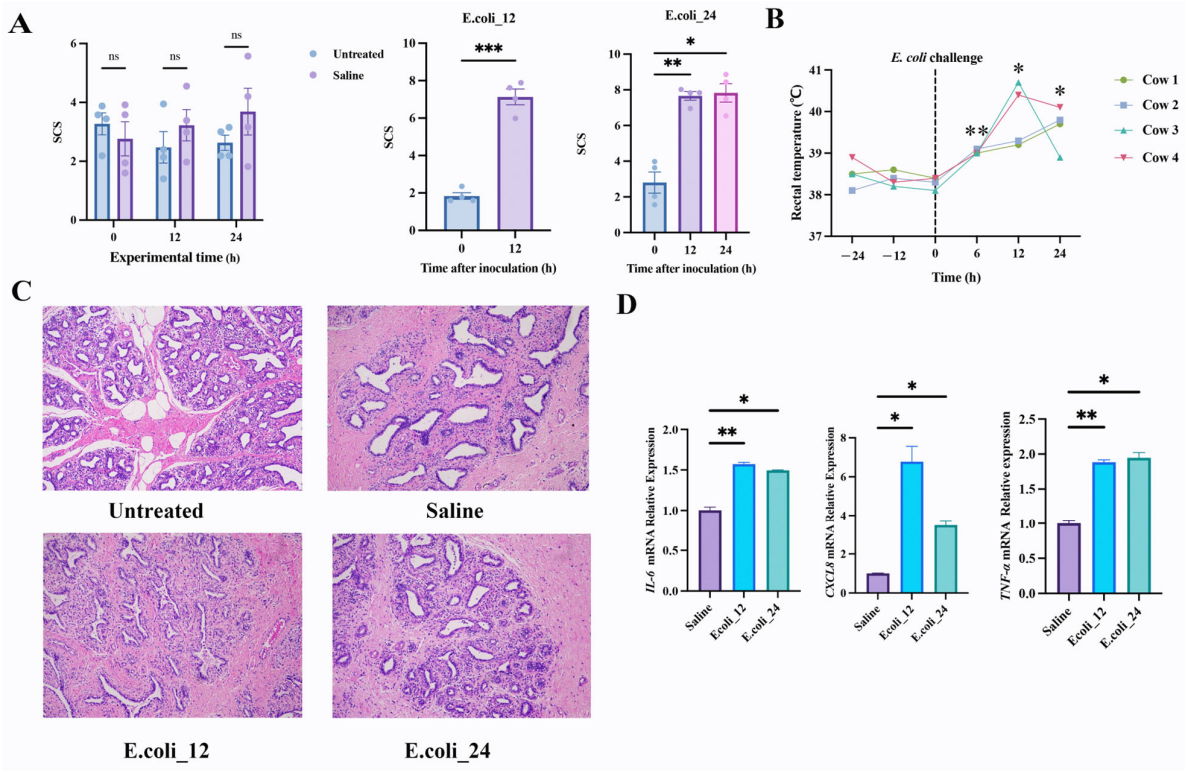


Figure 2. Inflammatory and histopathological responses following intramammary *Escherichia coli* challenge. (**A**) Somatic cell score (SCS) in untreated, saline-treated, and *E. coli*-challenged mammary quarters. (**B**) Rectal temperature before and after *E. coli* challenge. (**C**) Representative H&E-stained sections of mammary tissues from the untreated, saline, E. coli_12, and E. coli_24 groups. (**D**) Relative mRNA expression of *IL-6*, *CXCL8*, and *TNF-α* in mammary tissues. Data are presented as mean ± SEM. ns, $p \geq 0.05$; * $p < 0.05$; ** $p < 0.01$; *** $p < 0.001$.

3.2. Sequencing Quality Assessment

A total of 24 libraries, including 12 input libraries and 12 m6A-immunoprecipitated (IP) libraries, were constructed and sequenced. The 150-bp paired-end sequencing generated 34.12–52.21 million raw reads per library, corresponding to 5.12–7.83 Gb of raw data. After quality filtering, 33.07–50.54 million valid reads were retained per library, with valid data yields ranging from 4.56 to 7.03 Gb. The proportion of valid bases ranged from 81.93% to 93.27%. Across all libraries, Q20 and Q30 values ranged from 97.76% to 98.65% and from 94.45% to 96.08%, respectively, while GC content ranged from 50.50% to 56.96% (Table 2). These results indicated consistently high sequencing quality across the libraries and provided suitable data for subsequent analyses.

Table 2. Statistics of bases/reads information before and after filtration.

Sample_ID	Raw_Reads	Raw_Bases	Valid_Reads	Valid_Bases	Valid%	Q20%	Q30%	GC%
Saline_1_IP	391,52316	5.87G	379,43752	5.48G	93.23	98.57	95.81	51.72
Saline_2_IP	367,30492	5.51G	353,15676	4.90G	89.02	98.25	95.39	53.78
Saline_3_IP	416,92282	6.25G	404,84616	5.71G	91.32	98.38	95.38	52.87
Saline_4_IP	493,08754	7.40G	474,59612	6.74G	91.15	98.31	95.38	53.86
E. coli_12_1_IP	460,58042	6.91G	444,86264	6.19G	89.66	98.50	95.79	50.50
E. coli_12_2_IP	509,23250	7.64G	492,01810	6.88G	90.02	98.47	95.59	52.58
E. coli_12_3_IP	522,05174	7.83G	505,40354	7.03G	89.73	98.52	95.76	51.78

Table 2. *Cont.*

Sample_ID	Raw_Reads	Raw_Bases	Valid_Reads	Valid_Bases	Valid%	Q20%	Q30%	GC%
E. coli_12_4_IP	425,55816	6.38G	410,89704	5.78G	90.52	98.46	95.58	52.60
E. coli_24_1_IP	355,56096	5.33G	343,52082	4.79G	89.87	98.42	95.71	53.66
E. coli_24_2_IP	389,93420	5.85G	379,35246	5.46G	93.27	98.65	96.08	52.10
E. coli_24_3_IP	341,16362	5.12G	330,66670	4.65G	90.80	98.56	95.87	51.69
E. coli_24_4_IP	381,05994	5.72G	369,50666	5.18G	90.69	98.56	96.02	53.69
Saline_1_input	404,23032	6.06G	384,20552	5.36G	88.37	97.98	94.65	55.34
Saline_2_input	359,94284	5.40G	343,03868	4.56G	84.37	97.83	94.48	56.20
Saline_3_input	415,74066	6.24G	395,65606	5.37G	86.18	97.89	94.53	55.98
Saline_4_input	400,27698	6.00G	383,14254	5.11G	85.06	98.01	94.81	56.51
E. coli_12_1_input	414,78258	6.22G	395,60984	5.10G	81.93	97.76	94.45	56.96
E. coli_12_2_input	420,70292	6.31G	402,62094	5.50G	87.20	98.08	94.82	55.23
E. coli_12_3_input	385,66588	5.78G	368,39786	5.03G	86.96	98.05	94.79	55.71
E. coli_12_4_input	454,61978	6.82G	433,52904	5.84G	85.65	98.02	94.69	55.22
E. coli_24_1_input	356.19288	5.34G	342,66026	4.59G	85.99	98.14	95.17	55.21
E. coli_24_2_input	419,65256	6.29G	402,26028	5.49G	87.14	98.11	94.96	55.43
E. coli_24_3_input	503,64652	7.55G	478,94480	6.54G	86.63	97.91	94.58	55.48
E. coli_24_4_input	421,86330	6.33G	404,47640	5.54G	87.52	98.17	95.10	55.47

3.3. Reference Genomic Alignment

Quality-filtered reads were aligned to the bovine reference genome (ARS-UCD2.0). Across the 24 libraries, 75.75–88.85% of valid reads were mapped to the reference genome, of which 69.84–83.77% were uniquely mapped, while 4.01–11.14% were mapped to multiple genomic locations (Table 3). Most mapped reads were assigned to exonic regions, whereas smaller proportions were mapped to intronic and intergenic regions (Figure 3).

Table 3. Alignment of bovine reference genome statistics.

Sample_ID	Valid Reads	Mapped Reads	Unique Mapped Reads	Multi Mapped Reads
Saline_1_IP	376,43966	330,89631 (87.90%)	315,34869 (83.77%)	15,54762 (4.13%)
Saline_2_IP	351,22150	266,05070 (75.75%)	245,30573 (69.84%)	20,74497 (5.91%)
Saline_3_IP	401,84438	332l43897 (82.73%)	311,47198 (77.51%)	20,96699 (5.22%)
Saline_4_IP	471,47308	393,78128 (83.52%)	367,07367 (77.86%)	26,70761 (5.66%)
E. coli_12_1_IP	440,48376	379,96521 (86.26%)	359,70705 (81.66%)	20,25816 (4.60%)
E. coli_12_2_IP	489,98256	424,17886 (86.57%)	403,69557 (82.39%)	20,48329 (4.18%)
E. coli_12_3_IP	502,22062	435,91135 (86.80%)	412,76284 (82.19%)	23,14851 (4.61%)
E. coli_12_4_IP	408,50890	359,25461 (87.94%)	338,05073 (82.75%)	21,20388 (5.19%)
E. coli_24_1_IP	341,71440	265,93167 (77.82%)	249,83840 (73.11%)	16,09327 (4.71%)
E. coli_24_2_IP	376,24782	322,49402 (85.71%)	307,41124 (81.70%)	15,08278 (4.01%)
E. coli_24_3_IP	326,93174	285,91739 (87.45%)	268,77599 (82.21%)	17,14140 (5.24%)
E. coli_24_4_IP	367,68908	316,75697 (86.15%)	299,65970 (81.50%)	17,09727 (4.65%)
Saline_1_input	378,71010	335,05331 (88.47%)	303,28562 (80.08%)	31,76769 (8.39%)
Saline_2_input	338,53804	288,92045 (85.34%)	252,75447 (74.66%)	36,16598 (10.68%)
Saline_3_input	389,49650	335,14704 (86.05%)	297,03790 (76.26%)	38,10914 (9.78%)
Saline_4_input	377,83762	325,89462 (86.25%)	283,79330 (75.11%)	42,10132 (11.14%)
E. coli_12_1_input	390,94348	329,44577 (84.27%)	288,51511 (73.80%)	40,93066 (10.47%)
E. coli_12_2_input	397,91142	350,82453 (88.17%)	317,59657 (79.82%)	33,22796 (8.35%)
E. coli_12_3_input	363,29792	319,61914 (87.98%)	286,08563 (78.75%)	33,53351 (9.23%)
E. coli_12_4_input	428,91850	375,94789 (87.65%)	338,90409 (79.01%)	37,04380 (8.64%)
E. coli_24_1_input	339,44454	295,46854 (87.04%)	264,69981 (77.98%)	30,76873 (9.06%)
E. coli_24_2_input	398,62286	350,30155 (87.88%)	315,15645 (79.06%)	35,14510 (8.82%)
E. coli_24_3_input	474,09392	415,43095 (87.63%)	373,53594 (78.79%)	41,89501 (8.84%)
E. coli_24_4_input	400,21236	355,58367 (88.85%)	318,17890 (79.50%)	37,40477 (9.35%)

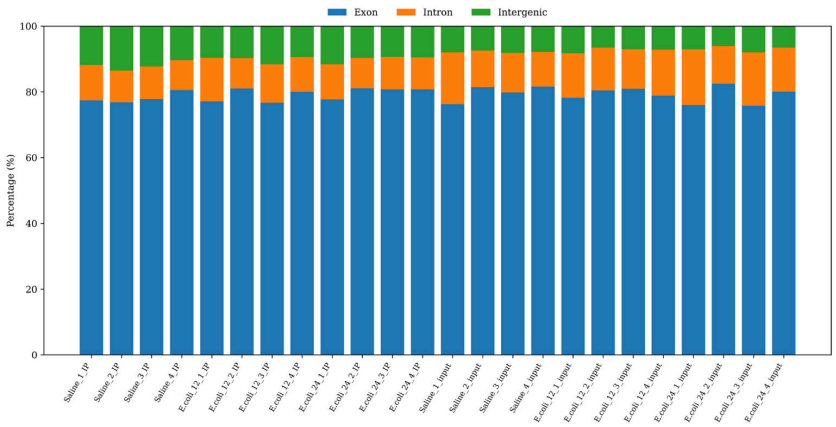


Figure 3. Genomic distribution of MeRIP-seq reads. The proportions of reads mapped to exonic, intronic, and intergenic regions in each sequencing library are shown as a 100% stacked bar chart.

3.4. Distribution of m6A Peaks Across Transcript Regions

The distribution of identified m6A peaks across transcript regions was examined in the Saline, E. coli_12, and E. coli_24 groups. A similar overall distribution pattern was observed among the three groups. The largest proportion of m6A peaks was located in the CDS (38.0–41.5%), followed by the stop-codon region (25.0–26.3%) and 3′UTR (18.2–19.1%), whereas relatively smaller proportions were located in the start-codon region (10.2–12.6%) and 5′UTR (4.0–5.0%) (Figure 4A–C). The density profiles also showed a broadly similar distribution pattern across transcript regions among the three groups (Figure 4D).

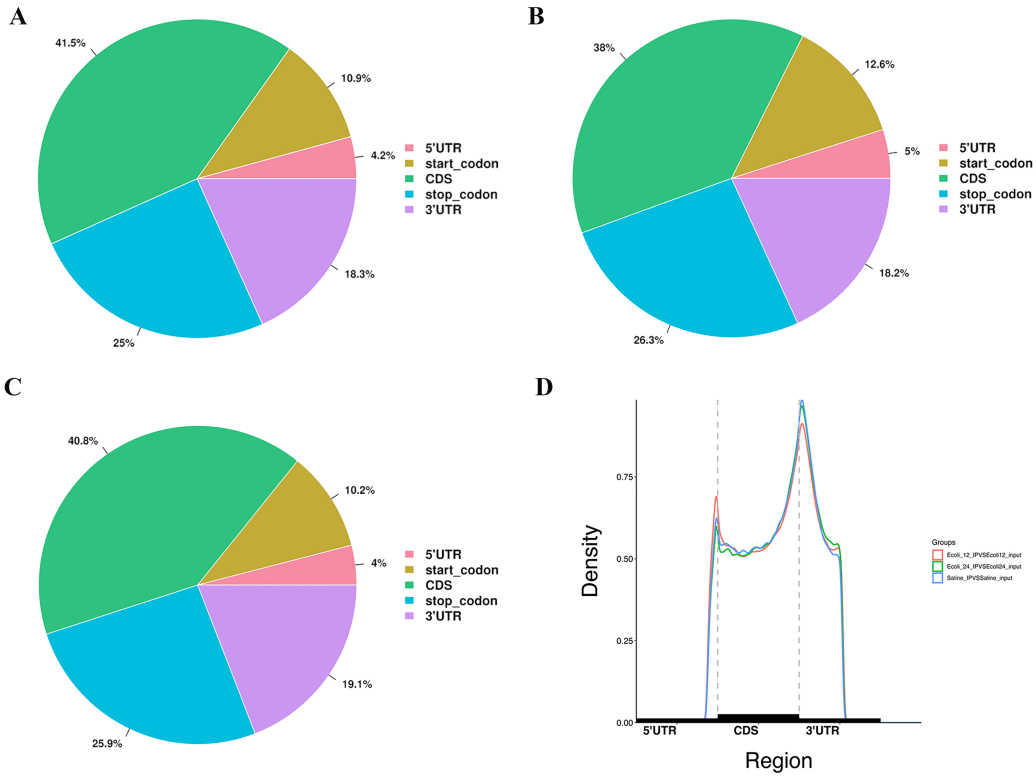


Figure 4. Distribution of m6A peaks across transcript regions. (**A**–**C**) Proportional distribution of identified m6A peaks across the 5′UTR, start codon, CDS, stop codon, and 3′UTR regions in the Saline, E. coli_12, and E. coli_24 groups, respectively. (**D**) Density distribution of m6A peaks across transcript regions in the three groups.

3.5. Differential m6A Peaks Analysis

Differential m6A enrichment was analyzed using a threshold of $|\log2FC| \geq 1$ and FDR < 0.05. Compared with the Saline group, 2242 differential m6A peaks were identified in the E. coli_12 group, including 1543 hyper-enriched and 699 hypo-enriched peaks (Figure 5A). In the E. coli_24 versus Saline comparison, 1848 differential peaks were identified, comprising 1255 hyper-enriched and 593 hypo-enriched peaks (Figure 5B). Comparison of the E. coli_12 and E. coli_24 groups identified 3826 differential peaks, including 1848 hyper-enriched and 1978 hypo-enriched peaks (Figure 5C). The top five hyper-enriched and top five hypo-enriched peaks for each comparison are summarized in Tables 4–6.

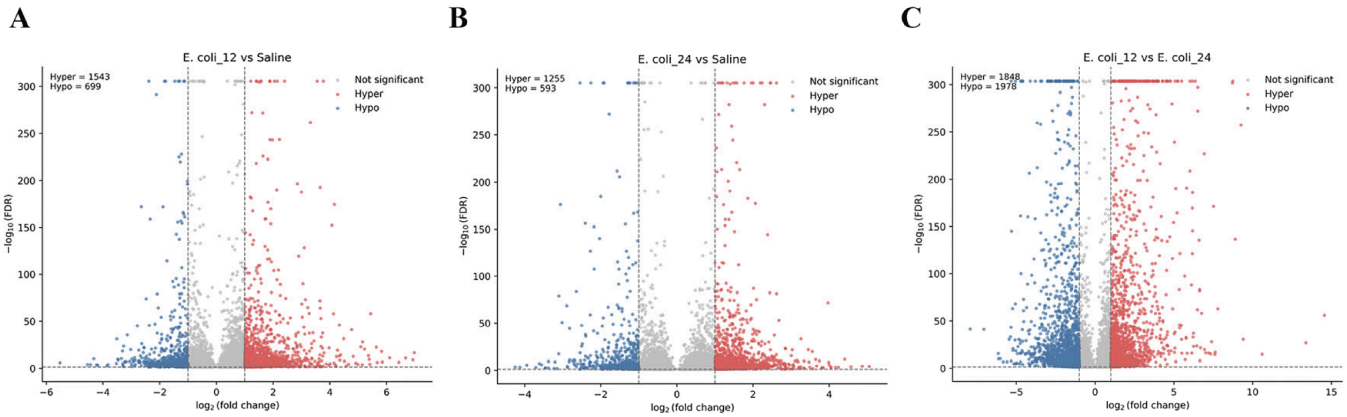


Figure 5. Volcano plots of differential m6A enrichment among the experimental groups. (**A**) E. coli_12 vs. Saline. (**B**) E. coli_24 vs. Saline. (**C**) E. coli_12 vs. E. coli_24. Red and blue points indicate hyper-enriched and hypo-enriched m6A peaks, respectively, whereas gray points indicate peaks that did not meet the significance criteria.

Table 4. Top 10 differential m6A peaks in E. coli_12 vs. Saline.

Gene	Chromosome	Peak Region	$\log_2$FC	FDR (q Value)	Regulation
CYP3A4	chr25	stop_codon	6.982	4.84×10^{-17}	Hyper
ODAM	chr6	exonic	6.935	1.30×10^{-9}	Hyper
PGLYRP2	chr7	exonic	6.674	1.92×10^{-11}	Hyper
TNIP3	chr17	3′UTR	6.436	6.21×10^{-7}	Hyper
SLC6A14	X	exonic	6.111	1.40×10^{-11}	Hyper
SCN3B	chr15	3′UTR	−5.515	1.82×10^{-6}	Hypo
LRRC66	chr6	exonic	−4.544	1.13×10^{-4}	Hypo
ZNF449	X	exonic	−4.438	1.75×10^{-4}	Hypo
FUT6	chr7	3′UTR	−4.321	1.28×10^{-10}	Hypo
ILDR2	chr3	3′UTR	−4.226	3.51×10^{-4}	Hypo

Table 5. Top 10 differential m6A peaks in the E. coli_24 vs. Saline comparison.

Gene	Chromosome	Peak Region	$\log_2$FC	FDR (q Value)	Regulation
SLITRK5	chr12	exonic	5.053	6.32×10^{-5}	Hyper
ALDH1B1	chr8	exonic	4.867	3.96×10^{-5}	Hyper
ZSCAN30	chr24	exonic	4.572	1.50×10^{-4}	Hyper
RSPO3	chr9	stop_codon	4.406	1.74×10^{-12}	Hyper
AMOTL1	chr15	5′UTR	4.242	4.81×10^{-4}	Hyper
ENSBTAG00000049346	chr18	exonic	−4.249	3.29×10^{-4}	Hypo
LRRC66	chr6	exonic	−4.125	4.74×10^{-4}	Hypo
IL4I1	chr18	exonic	−3.941	3.55×10^{-6}	Hypo
ENSBTAG00000049888	chr15	ncRNA_exonic	−3.707	9.14×10^{-4}	Hypo
TNFSF18	chr16	stop_codon	−3.612	6.57×10^{-8}	Hypo

Table 6. Top 10 differential m6A peaks in the E. coli_12 vs. E. coli_24 comparison.

Gene	Chromosome	Peak Region	$\log_2$FC	FDR (q Value)	Regulation
PGLYRP2	chr7	exonic	14.554	9.91×10^{-57}	Hyper
ENSBTAG00000054882	chr24	exonic	13.381	2.41×10^{-27}	Hyper
KLK10	chr18	3′UTR	10.606	2.95×10^{-15}	Hyper
PSORS1C2	chr23	exonic	9.404	4.62×10^{-31}	Hyper
TNIP3	chr17	exonic	9.257	5.02×10^{-258}	Hyper
RSPO3	chr9	stop_codon	−7.923	5.43×10^{-42}	Hypo
RSPO3	chr9	3′UTR	−7.054	1.09×10^{-41}	Hypo
IGSF10	chr1	exonic	−6.137	4.82×10^{-16}	Hypo
PLIN4	chr7	exonic	−6.123	1.61×10^{-10}	Hypo
BCHE	chr1	exonic	−6.011	9.76×10^{-11}	Hypo

3.6. Functional Enrichment Analysis of Differential Peaks

GO enrichment analysis showed that genes associated with differential m6A peaks were mainly enriched in biological processes related to inflammatory and immune responses, cytokine production, cell adhesion, and signal transduction (Figure 6). KEGG analysis further revealed significant enrichment of several inflammation- and immune-related pathways, including the NF-κB, TNF, MAPK, chemokine, and NOD-like receptor signaling pathways (Figure 7). Overall, these results indicate that differential m6A enrichment following *E. coli* challenge was primarily associated with inflammatory and immune-related biological processes and signaling pathways.

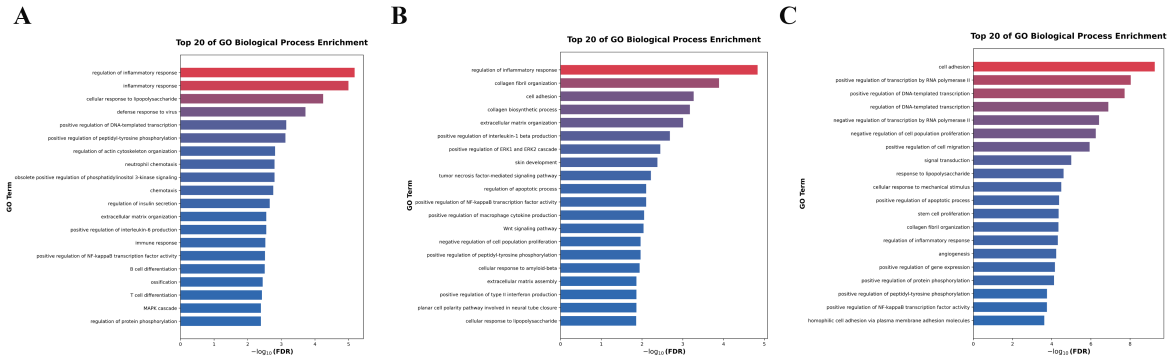


Figure 6. GO biological process enrichment analysis of genes associated with differential m6A peaks. (**A**) E. coli_12 vs. Saline. (**B**) E. coli_24 vs. Saline. (**C**) E. coli_12 vs. E. coli_24. Only significantly enriched GO terms with FDR <0.05 are shown.

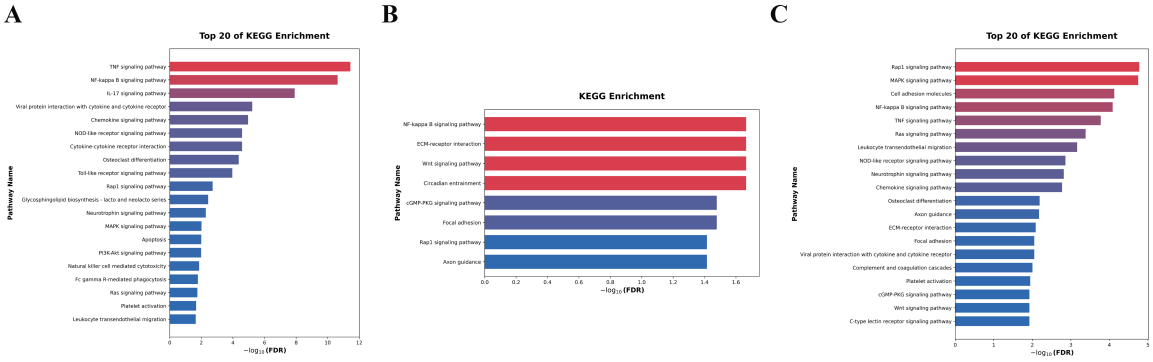


Figure 7. KEGG pathway enrichment analysis of genes associated with differential m6A peaks. (**A**) E. coli_12 vs. Saline. (**B**) E. coli_24 vs. Saline. (**C**) E. coli_12 vs. E. coli_24. Only significantly enriched KEGG pathways with FDR <0.05 are shown.

3.7. Motif Analysis

Motif enrichment analysis identified several significantly enriched sequence motifs within m6A peak regions in the Saline, E. coli_12, and E. coli_24 groups (Figure 8). The top five motifs in each group showed strong enrichment. Several similar sequence patterns were observed across the three groups, suggesting shared sequence characteristics of m6A-enriched regions.

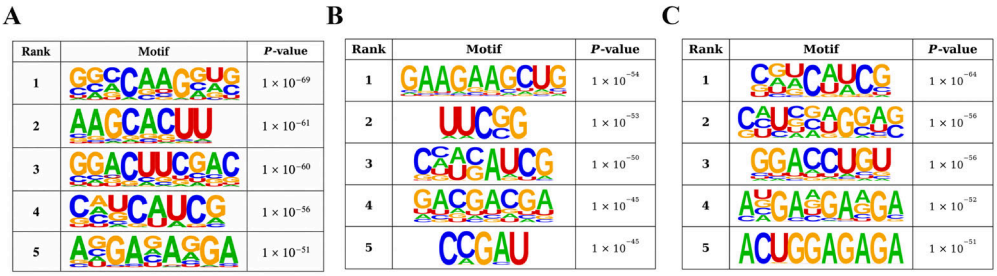


Figure 8. The top five enriched sequence motifs identified within m6A peak regions in the Saline (**A**), E. coli_12 (**B**), and E. coli_24 (**C**) groups are shown. Motifs were ranked according to enrichment significance.

3.8. RNA-Seq Analysis

Differentially expressed genes (DEGs) were identified using the criteria of $|\log2FC| \geq 1$ and FDR < 0.05. Compared with the saline group, 591 DEGs were identified in the E. coli_12 group, including 425 upregulated and 166 downregulated genes (Figure 9). In the E. coli_24 group, 1287 DEGs were identified compared with the saline group, of which 717 were upregulated and 570 were downregulated. Comparison between the E. coli_12 and E. coli_24 groups identified 554 DEGs, including 317 upregulated and 237 downregulated genes (Figure 9). PCA and sample correlation analyses were performed to evaluate the overall similarity and variation among the RNA-seq samples. The samples showed generally high correlations, while PCA revealed both treatment-related variation and inter-individual variation among cows (Figure S1).

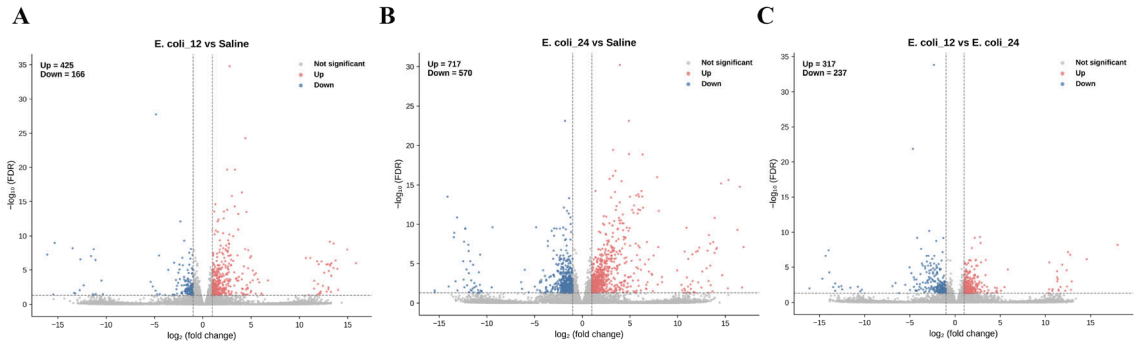


Figure 9. Volcano plots of differentially expressed genes (DEGs) in the three comparison groups. (**A**) E. coli_12 vs. Saline. (**B**) E. coli_24 vs. Saline. (**C**) E. coli_12 vs. E. coli_24.

GO enrichment analysis showed that differentially expressed genes (DEGs) were mainly enriched in biological processes related to immune and inflammatory responses, neutrophil chemotaxis, cell migration, and responses to bacterial stimuli (Figure 10). KEGG analysis further revealed significant enrichment of inflammation- and immune-related pathways, including cytokine–cytokine receptor interaction, chemokine, IL-17, NOD-like receptor, NF-κB, and TNF signaling pathways (Figure 11). These results indicate that the transcriptional response to *E. coli* challenge was predominantly associated with inflammatory and innate immune processes.

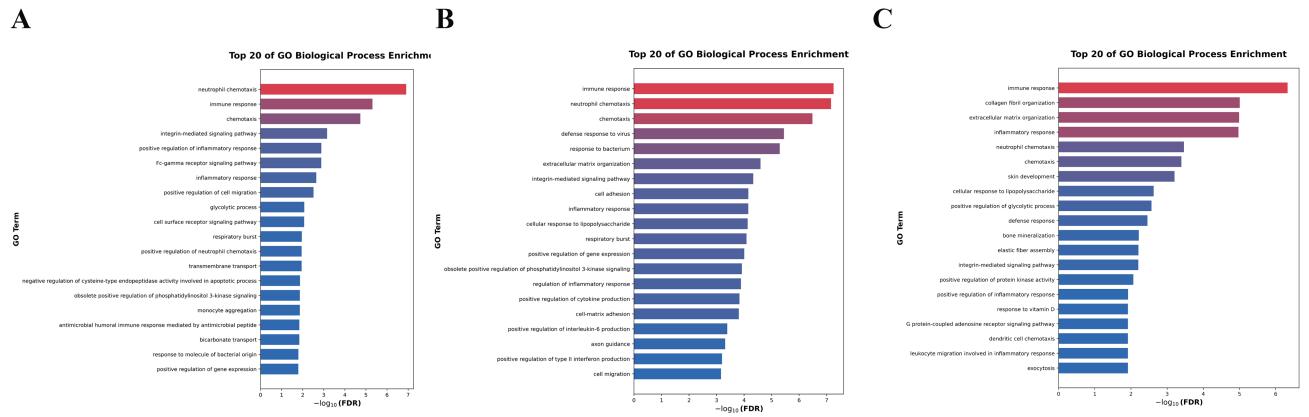


Figure 10. GO biological process enrichment analysis of differentially expressed genes. (**A**) E. coli_12 vs. Saline. (**B**) E. coli_24 vs. Saline. (**C**) E. coli_12 vs. E. coli_24. Only significantly enriched GO terms with FDR <0.05 are shown.

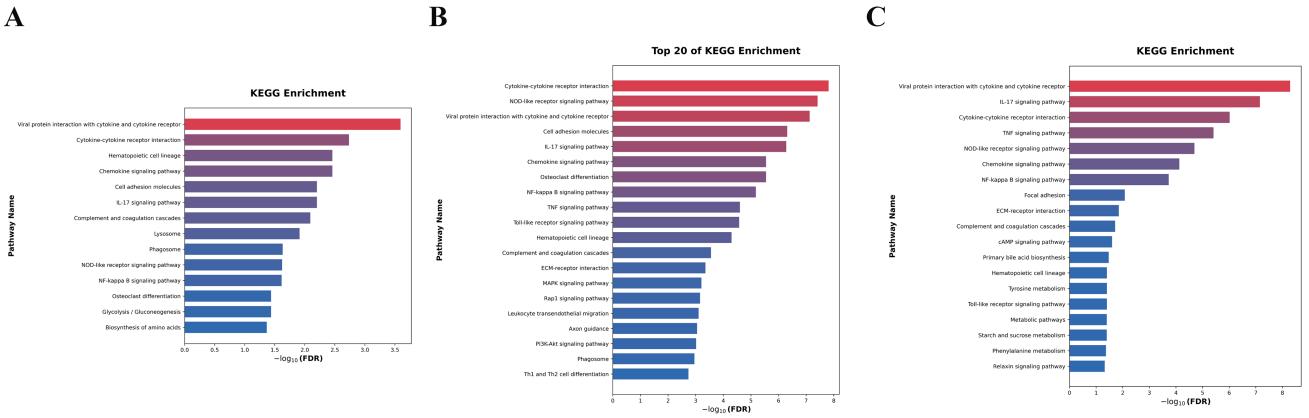


Figure 11. KEGG pathway enrichment analysis of differentially expressed genes. (**A**) E. coli_12 vs. Saline. (**B**) E. coli_24 vs. Saline. (**C**) E. coli_12 vs. E. coli_24. Only significantly enriched KEGG pathways with FDR <0.05 are shown.

3.9. Integrated Analysis of MeRIP-Seq and RNA-Seq

Integrated analysis of MeRIP-seq and RNA-seq data was performed to examine the association between m6A enrichment and gene expression (Figure 12). In E. coli_12 versus Saline, 264 differentially m6A peak-gene associations were identified, predominantly Hyper-Up pairs (192). In E. coli_24 versus Saline, 476 differential m6A peak-gene associations were identified, mainly Hyper-Down (280) and Hypo-Up (190). In E. coli_12 versus E. coli_24, 459 differential m6A peak-gene associations were identified, consisting primarily of Hypo-Up (234) and Hyper-Down (225) pairs.

GO enrichment analysis showed differential m6A peak-gene associations were mainly enriched in immune and inflammatory responses, neutrophil chemotaxis, chemotaxis, extracellular matrix organization, and responses to bacterial stimuli (Figure 13). KEGG analysis further showed enrichment in inflammation- and immune-related pathways, including IL-17, NF-κB, chemokine, cytokine–cytokine receptor interaction, NOD-like receptor, and TNF signaling pathways (Figure 14).

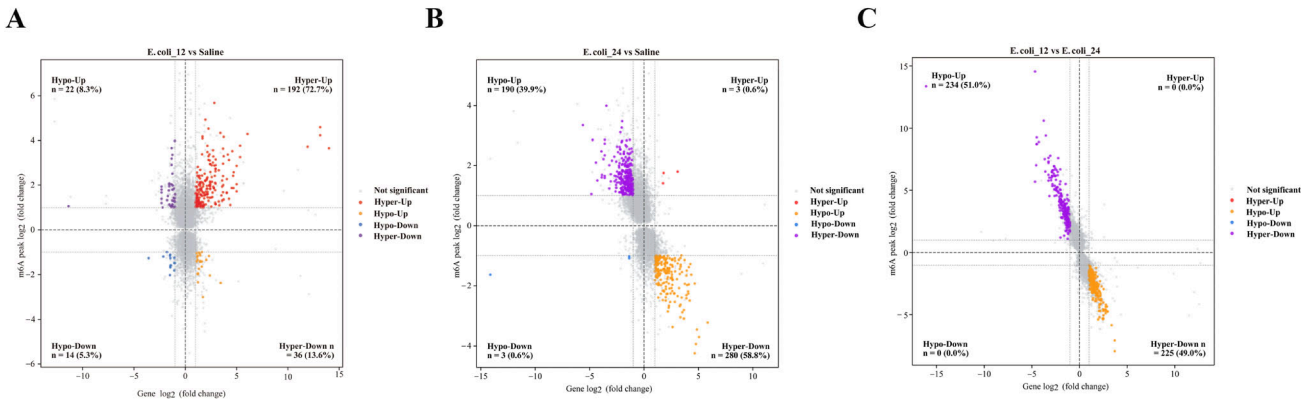


Figure 12. Integrated analysis of differential m6A methylation and gene expression. (**A**–**C**) Overlap of genes with significant changes in both m6A modification and gene expression in the three comparison groups, respectively.

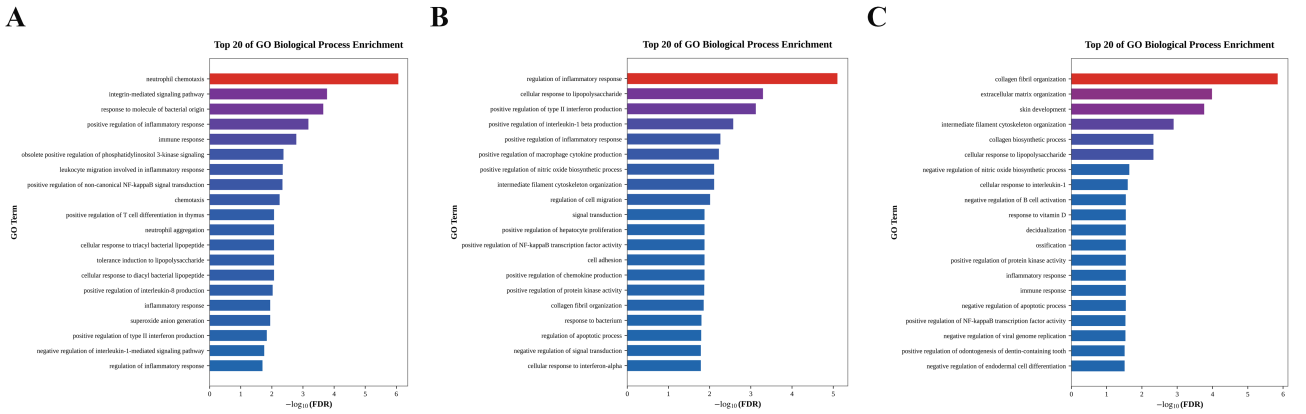


Figure 13. GO biological process enrichment analysis of differential m6A peak-gene associations. (**A**) E. coli_12 vs. Saline. (**B**) E. coli_24 vs. Saline. (**C**) E. coli_12 vs. E. coli_24. Only significantly enriched GO terms with FDR <0.05 are shown.

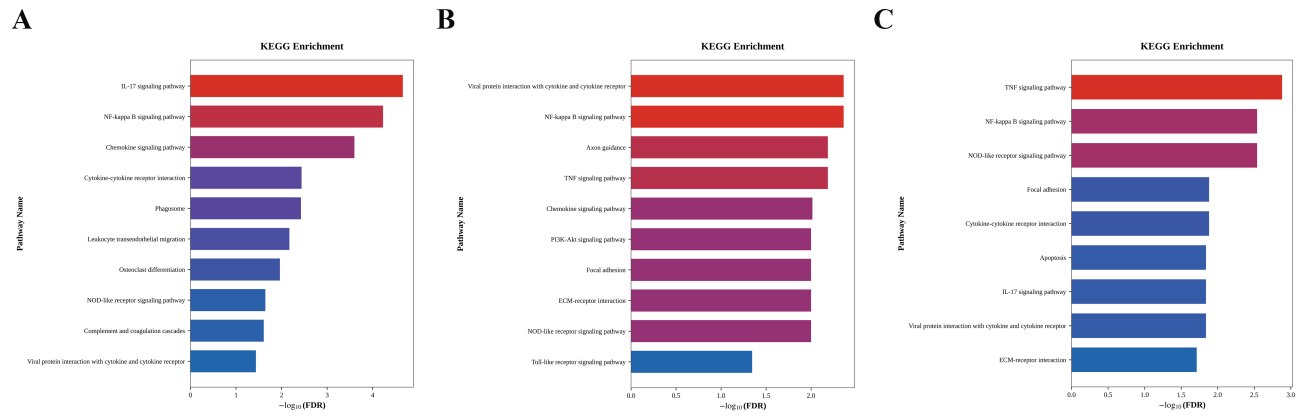


Figure 14. KEGG pathway enrichment analysis of differential m6A peak-gene associations. (**A**) E. coli_12 vs. Saline. (**B**) E. coli_24 vs. Saline. (**C**) E. coli_12 vs. E. coli_24. Only significantly enriched KEGG pathways with FDR <0.05 are shown.

4. Discussion

N6-methyladenosine (m6A) is an important RNA modification involved in post-transcriptional regulation and has been associated with inflammatory and immune responses [4–8]. In this study, MeRIP-seq and RNA-seq were used to characterize m6A

methylation and gene expression in bovine mammary tissues following intramammary *Escherichia coli* challenge. Changes in both m6A methylation and gene expression were observed after challenge, and the 12 h and 24 h exposure groups showed different response patterns. However, because a staggered within-cow inoculation design was used, differences between the two exposure groups may be related not only to local exposure duration but also to prior systemic inflammatory exposure.

RNA-seq analysis showed differences between the 12 h and 24 h exposure groups. Many of the DEGs were related to inflammatory and immune responses. GO and KEGG analyses showed enrichment of neutrophil chemotaxis, cytokine-mediated signaling, and NOD-like receptor signaling. These processes have also been reported in *E. coli*-induced bovine mastitis [30–32]. Neutrophil recruitment is an important part of the early mammary response to *E. coli* infection and contributes to bacterial clearance [20,33,34]. The number and functional distribution of DEGs differed between the two exposure groups. However, these differences may be related to both local exposure duration and the systemic effects of the staggered inoculation design.

Functional enrichment analysis showed that differential m6A peaks were involved in several immune- and inflammation-related processes. GO terms related to the extracellular region and extracellular space were enriched in multiple comparisons, together with terms associated with chemokine activity and immune responses. KEGG analysis identified cytokine–cytokine receptor interaction, NOD-like receptor, IL-17, TNF, MAPK, and NF-κB signaling pathways, several of which have previously been linked to bovine mastitis [20,35,36]. The enrichment of these pathways suggests that changes in m6A methylation occurred in genes related to the mammary immune response to *E. coli*. However, these results show functional associations and do not provide direct evidence that m6A methylation regulates the activity of these pathways.

Consistent with previous studies, m6A peaks were mainly distributed in CDS regions and around stop codons, and similar sequence motifs were found across the three groups [2–5]. Integration of MeRIP-seq and RNA-seq further identified genes showing both differential m6A enrichment and differential gene expression. Differential MeRIP enrichment was interpreted relative to matched input abundance, considering the limitations of distinguishing methylation changes from expression changes described by McIntyre et al. [37]. The integrated results showed that changes in m6A enrichment were accompanied by changes in transcript abundance in a subset of inflammation-related genes. However, the direction of these changes was not uniform across genes or comparisons, indicating that the relationship between m6A enrichment and gene expression may be context dependent. Therefore, the present data support an association between m6A enrichment and transcriptional responses rather than a direct regulatory relationship. Moreover, differences in enrichment profiles between separate comparisons should not be interpreted as statistically significant differences between exposure groups.

Several inflammation-related genes showed changes in both m6A enrichment and gene expression. In the 12 h exposure group, *CXCL8*, *IL1B*, and *TNFAIP3* showed increased m6A enrichment together with increased gene expression. In contrast, *TNF*, *TLR2*, and *NFKBIA* showed reduced m6A enrichment but increased gene expression in the 24 h exposure group. These genes are involved in inflammatory and innate immune responses and have been associated with the mammary response to bacterial infection [38–43]. The different patterns observed between m6A enrichment and gene expression indicate that their relationship may vary among genes and exposure groups. Further validation is needed to determine whether the observed m6A changes are related to the expression of these genes during mammary inflammation. Recent studies in ruminants further indicate that inflammatory responses are accompanied by coordinated changes across multiple biological processes. In goats,

modulation of inflammatory cytokines has been associated with changes in antioxidant status and rumen microbial composition [44]. Moreover, an integrated multi-omics study demonstrated coordinated alterations in inflammatory responses, microbial composition, and host metabolic pathways [45]. These findings highlight the value of integrating multiple molecular layers when investigating inflammatory responses in ruminants. In the present study, the integration of MeRIP-seq and RNA-seq similarly provided complementary information on changes in m6A enrichment and transcript abundance. Nevertheless, functional experiments are required to determine whether these molecular changes are mechanistically linked.

This study has several limitations. The staggered within-cow inoculation design may have resulted in systemic pre-exposure and order effects, and responses induced in the challenged quarters may also have influenced the control quarters. Differences between the 12 h and 24 h exposure groups therefore cannot be explained by exposure duration alone. The experiment was conducted in four cows using a laboratory reference strain of *E. coli*, which may not fully represent naturally occurring mastitis. Although the cows were clinically healthy and mammary-quarter SCC was monitored before challenge, pre-challenge bacteriological culture was not performed. In addition, the changes in m6A enrichment identified by MeRIP-seq were not further validated by MeRIP-qPCR. These limitations should be taken into account when interpreting the results.

5. Conclusions

This study characterized m6A enrichment and transcriptomic responses in bovine mammary tissue following intramammary *E. coli* challenge using a within-cow mammary-quarter design. After accounting for cow identity, differential m6A enrichment and gene expression were identified in both the 12 h and 24 h exposure groups compared with the saline control, with immune- and inflammation-related biological processes represented among the significantly enriched results. Integrated analysis further identified genes showing both differential m6A enrichment and differential expression. These findings indicate an association between m6A enrichment and transcriptional responses during *E. coli*-induced mammary inflammation but do not establish a direct regulatory relationship. Because of the staggered challenge design and common tissue-sampling endpoint, differences between the 12 h and 24 h exposure groups should not be interpreted as a simple temporal progression.

Supplementary Materials: The following supporting information can be downloaded at: https://www.mdpi.com/article/10.3390/vetsci13111192/s1, Figure S1: Principal component and correlation analyses of RNA-seq samples. (A) Principal component analysis (PCA) of RNA-seq samples. (B) Pearson correlation heatmap of RNA-seq samples.

Author Contributions: Conceptualization, Y.W. and Y.M.; methodology, Y.W. and Y.M.; software, Y.W.; validation, Y.W.; formal analysis, Y.W.; investigation, Y.W.; resources, Y.M.; data curation, Y.W.; writing—original draft preparation, Y.W.; writing—review and editing, Y.W., H.Z., M.L., N.A.K. and Y.M.; visualization, Y.W.; supervision, H.Z., M.L. and N.A.K.; project administration, Y.M.; funding acquisition, Y.M. All authors have read and agreed to the published version of the manuscript.

Funding: This study was supported by the National Natural Science Foundation of China (31972555), the Jiangsu Provincial Frontier Technology Research and Development Program (Modern Agriculture) (BF20260305) and Jiangsu Province Graduate Research and Practice Innovation Program (KYCX24-3804).

Institutional Review Board Statement: All animal experimental procedures were reviewed and approved by the Animal Welfare and Ethics Committee of Yangzhou University (Approval No. 202303016; approved on 2 March 2023). The experimental animals were provided by Xuzhou Meizi

Ke Animal Husbandry Technology Co., Ltd., and informed consent for the use of animals in this scientific study was obtained through an animal use agreement between Yangzhou University and the farm.

Informed Consent Statement: Informed consent was obtained from all subjects involved in the study.

Data Availability Statement: The datasets presented in this article are not readily available because the raw RNA-seq and MeRIP-seq data, together with the relevant processed data, are currently undergoing deposition in a public repository (e.g., GEO/SRA/ENA), and the corresponding accession numbers will be released once the data deposition is completed. Requests to access the datasets should be directed to the corresponding author.

Conflicts of Interest: The authors declare no conflicts of interest.

References

1. Wei, C.M.; Gershowitz, A.; Moss, B. Methylated nucleotides block 5′ terminus of HeLa cell messenger RNA. *Cell* **1975**, *4*, 379–386. [CrossRef] [PubMed]
2. Wang, X.; Feng, J.; Xue, Y.; Guan, Z.; Zhang, D.; Liu, Z.; Gong, Z.; Wang, Q.; Huang, J.; Tang, C.; et al. Structural basis of N^6-adenosine methylation by the METTL3-METTL14 complex. *Nature* **2016**, *534*, 575–578. [CrossRef] [PubMed]
3. Zheng, G.; Dahl, J.A.; Niu, Y.; Fedorcsak, P.; Huang, C.M.; Li, C.J.; Vågbø, C.B.; Shi, Y.; Wang, W.L.; Song, S.H.; et al. ALKBH5 is a mammalian RNA demethylase that impacts RNA metabolism and mouse fertility. *Mol. Cell* **2013**, *49*, 18–29. [CrossRef] [PubMed]
4. Shi, H.; Wei, J.; He, C. Where, When, and How: Context-Dependent Functions of RNA Methylation Writers, Readers, and Erasers. *Mol. Cell* **2019**, *74*, 640–650. [CrossRef] [PubMed]
5. Zaccara, S.; Ries, R.J.; Jaffrey, S.R. Reading, writing and erasing mRNA methylation. *Nat. Rev. Mol. Cell Biol.* **2019**, *20*, 608–624. [CrossRef] [PubMed]
6. Li, Z.; Lao, Y.; Yan, R.; Li, F.; Guan, X.; Dong, Z. N6-methyladenosine in inflammatory diseases: Important actors and regulatory targets. *Gene* **2025**, *936*, 149125. [CrossRef] [PubMed]
7. Yu, J.; She, Y.; Ji, S.J. m (6)A Modification in Mammalian Nervous System Development, Functions, Disorders, and Injuries. *Front Cell Dev. Biol.* **2021**, *9*, 679662. [CrossRef] [PubMed]
8. Ma, W.; Wu, T. RNA m6A modification in liver biology and its implication in hepatic diseases and carcinogenesis. *Am. J. Physiol. Cell Physiol.* **2022**, *323*, C1190–C1205. [CrossRef] [PubMed]
9. Cui, L.; Ma, R.; Cai, J.; Guo, C.; Chen, Z.; Yao, L.; Wang, Y.; Fan, R.; Wang, X.; Shi, Y. RNA modifications: Importance in immune cell biology and related diseases. *Signal Transduct. Target. Ther.* **2022**, *7*, 334. [CrossRef] [PubMed]
10. Li, L.; Xia, X.; Yang, T.; Sun, Y.; Liu, X.; Xu, W.; Lu, M.; Cui, D.; Wu, Y. RNA methylation: A potential therapeutic target in autoimmune disease. *Int. Rev. Immunol.* **2024**, *43*, 160–177. [CrossRef] [PubMed]
11. Sharun, K.; Dhama, K.; Tiwari, R.; Gugjoo, M.B.; Yatoo, M.I.; Patel, S.K.; Pathak, M.; Karthik, K.; Khurana, S.K.; Singh, R.; et al. Advances in therapeutic and managemental approaches of bovine mastitis: A comprehensive review. *Vet. Q.* **2021**, *41*, 107–136. [CrossRef] [PubMed]
12. Lamanna, M.; Polizzi, G.; Vastolo, A.; Cavallini, D. Milking Process and Milking Technology. In *Encyclopedia of Livestock Medicine for Large Animal and Poultry Production*; Simoes, J., Ed.; Springer Nature: Cham, Switzerland, 2024; pp. 1–14.
13. Shaheen, M.; Ha, T. A Treatise on Bovine Mastitis: Disease and Disease Economics, Etiological Basis, Risk Factors, Impact on Human Health, Therapeutic Management, Prevention and Control Strategy. *Adv. Dairy Res.* **2016**, *4*, 150. [CrossRef]
14. Zaatout, N. An overview on mastitis-associated *Escherichia coli*: Pathogenicity, host immunity and the use of alternative therapies. *Microbiol. Res.* **2022**, *256*, 126960. [CrossRef] [PubMed]
15. Khatun, M.; Sørensen, P.; Jørgensen, H.B.; Sahana, G.; Sørensen, L.P.; Lund, M.S.; Ingvartsen, K.L.; Buitenhuis, A.J.; Vilkki, J.; Bjerring, M.; et al. Effects of Bos taurus autosome 9-located quantitative trait loci haplotypes on the disease phenotypes of dairy cows with experimentally induced *Escherichia coli* mastitis. *J. Dairy Sci.* **2013**, *96*, 1820–1833. [CrossRef] [PubMed]
16. Murinda, S.E.; Ibekwe, A.M.; Rodriguez, N.G.; Quiroz, K.L.; Mujica, A.P.; Osmon, K. Shiga Toxin-Producing *Escherichia coli* in Mastitis: An International Perspective. *Foodborne Pathog. Dis.* **2019**, *16*, 229–243. [CrossRef] [PubMed]
17. Abdi, R.D.; Gillespie, B.E.; Ivey, S.; Pighetti, G.M.; Almeida, R.A.; Kerro Dego, O. Antimicrobial Resistance of Major Bacterial Pathogens from Dairy Cows with High Somatic Cell Count and Clinical Mastitis. *Animals* **2021**, *11*, 131. [CrossRef] [PubMed]
18. Cobirka, M.; Tancin, V.; Slama, P. Epidemiology and Classification of Mastitis. *Animals* **2020**, *10*, 2212. [CrossRef] [PubMed]
19. Li, Y.; Zhu, Y.; Chu, B.; Liu, N.; Chen, S.; Wang, J.; Zou, Y. Map of Enteropathogenic *Escherichia coli* Targets Mitochondria and Triggers DRP-1-Mediated Mitochondrial Fission and Cell Apoptosis in Bovine Mastitis. *Int. J. Mol. Sci.* **2022**, *23*, 4907. [CrossRef] [PubMed]

20. Paape, M.; Mehrzad, J.; Zhao, X.; Detilleux, J.; Burvenich, C. Defense of the bovine mammary gland by polymorphonuclear neutrophil leukocytes. *J. Mammary Gland Biol. Neoplasia* **2002**, *7*, 109–121. [CrossRef] [PubMed]
21. Steimle, A.; Autenrieth, I.B.; Frick, J.S. Structure and function: Lipid A modifications in commensals and pathogens. *Int. J. Med. Microbiol.* **2016**, *306*, 290–301. [CrossRef] [PubMed]
22. Chen, W.; Liu, Y.; Yin, J.; Deng, Y.; Ali, T.; Zhang, J.; Cheng, J.; Ur Rahman, S.; Gao, J.; Han, B. Cloning, Expression, and Immunogenicity of Fimbrial-F17A Subunit Vaccine against *Escherichia coli* Isolated from Bovine Mastitis. *BioMed Res. Int.* **2017**, *2017*, 3248483. [CrossRef] [PubMed]
23. McConnel, C.S.; Crisp, S.A.; Biggs, T.D.; Ficklin, S.P.; Parrish, L.M.; Trombetta, S.C.; Sischo, W.M.; Adams-Progar, A. A Fixed Cohort Field Study of Gene Expression in Circulating Leukocytes From Dairy Cows With and Without Mastitis. *Front. Vet. Sci.* **2020**, *7*, 559279. [CrossRef] [PubMed]
24. Kempf, F.; Slugocki, C.; Blum, S.E.; Leitner, G.; Germon, P. Genomic Comparative Study of Bovine Mastitis *Escherichia coli*. *PLoS ONE* **2016**, *11*, e0147954. [CrossRef] [PubMed]
25. Mitterhuemer, S.; Petzl, W.; Krebs, S.; Mehne, D.; Klanner, A.; Wolf, E.; Zerbe, H.; Blum, H. *Escherichia coli* infection induces distinct local and systemic transcriptome responses in the mammary gland. *BMC Genom.* **2010**, *11*, 138. [CrossRef] [PubMed]
26. Nielsen, N.I.; Larsen, T.; Bjerring, M.; Ingvartsen, K.L. Quarter health, milking interval, and sampling time during milking affect the concentration of milk constituents. *J. Dairy Sci.* **2005**, *88*, 3186–3200. [CrossRef] [PubMed]
27. Bruckmaier, R.M.; Ontsouka, C.E.; Blum, J.W. Fractionized milk composition in dairy cows with subclinical mastitis. *Veterinární Medicína* **2004**, *49*, 283–290. [CrossRef]
28. Derakhshani, H.; Fehr, K.B.; Sepehri, S.; Francoz, D.; De Buck, J.; Barkema, H.W.; Plaizier, J.C.; Khafipour, E. Invited review: Microbiota of the bovine udder: Contributing factors and potential implications for udder health and mastitis susceptibility. *J. Dairy Sci.* **2018**, *101*, 10605–10625. [CrossRef] [PubMed]
29. Luoreng, Z.M.; Wang, J.P.; Jiao, P.; Li, Y.X.; Dong, Y.W.; Wei, D.W.; Wang, X.P. Construction of dairy cow mastitis model and analysis of mRNA transcription level of inflammation related cytokine genes. *Acta Vet. Zootech. Sin.* **2022**, *53*, 2763–2772. (In Chinese)
30. Iso-Touru, T.; Panitz, F.; Fischer, D.; Kyläniemi, M.K.; Taponen, S.; Tabell, J.; Virta, A.; Vilkki, J. Genes and pathways revealed by whole transcriptome analysis of milk derived bovine mammary epithelial cells after *Escherichia coli* challenge. *Vet. Res.* **2024**, *55*, 13. [CrossRef] [PubMed]
31. Zhang, K.; Zhang, Y.; Su, H.; Zhang, M.; Zhao, F.; Wang, D.; Cao, G.; Zhang, Y.; Wang, C. RNA Sequencing of Immune Response-Related Gene Expression Characteristics in Bovine Mammary Glands Infected with *Escherichia coli*. *Microorganisms* **2025**, *13*, 2226. [CrossRef] [PubMed]
32. Petzl, W.; Gunther, J.; Muhlbauer, K.; Seyfert, H.M.; Schuberth, H.J.; Hussen, J.; Sauter-Louis, C.; Hafner-Marx, A.; Zerbe, H. Early transcriptional events in the udder and teat after intra-mammary *Escherichia coli* and *Staphylococcus aureus* challenge. *Innate Immun.* **2016**, *22*, 294–304. [CrossRef] [PubMed]
33. Kremer, W.D.; Noordhuizen-Stassen, E.N.; Grommers, F.J.; Daemen, A.J.; Brand, A.; Burvenich, C. Blood polymorphonuclear leukocyte chemotaxis during experimental *Escherichia coli* bovine mastitis. *J. Dairy Sci.* **1993**, *76*, 2613–2618. [CrossRef] [PubMed]
34. Xie, L.; Ma, Y.; Opsomer, G.; Pascottini, O.B.; Guan, Y.; Dong, Q. Neutrophil extracellular traps in cattle health and disease. *Res. Vet. Sci.* **2021**, *139*, 4–10. [CrossRef] [PubMed]
35. Franchi, L.; Warner, N.; Viani, K.; Nunez, G. Function of Nod-like receptors in microbial recognition and host defense. *Immunol. Rev.* **2009**, *227*, 106–128. [CrossRef] [PubMed]
36. Wang, W.; Cheng, L.; Yi, J.; Gan, J.; Tang, H.; Fu, M.Z.; Wang, H.; Lai, S.J. Health and production traits in bovine are associated with single nucleotide polymorphisms in the *NOD2* gene. *Genet Mol. Res.* **2015**, *14*, 3570–3578. [CrossRef] [PubMed]
37. McIntyre, A.B.R.; Gokhale, N.S.; Cerchietti, L.; Jaffrey, S.R.; Horner, S.M.; Mason, C.E. Limits in the detection of m6A changes using MeRIP/m6A-seq. *Sci. Rep.* **2020**, *10*, 6590. [CrossRef] [PubMed]
38. Scalise, V.; Sanguinetti, C.; Neri, T.; Cianchetti, S.; Lai, M.; Carnicelli, V.; Celi, A.; Pedrinelli, R. *PCSK9* Induces Tissue Factor Expression by Activation of TLR4/NFkB Signaling. *Int. J. Mol. Sci.* **2021**, *22*, 12640. [CrossRef] [PubMed]
39. Che, H.Y.; Zhou, C.H.; Lyu, C.C.; Meng, Y.; He, Y.T.; Wang, H.Q.; Wu, H.Y.; Zhang, J.B.; Yuan, B. Allicin Alleviated LPS-Induced Mastitis via the TLR4/NF-κB Signaling Pathway in Bovine Mammary Epithelial Cells. *Int. J. Mol. Sci.* **2023**, *24*, 3805. [CrossRef] [PubMed]
40. Xu, H.; Lin, C.; Yang, J.; Chen, X.; Chen, Y.; Chen, J.; Guo, A.; Hu, C. The Role of N^6-Methyladenosine in Inflammatory Diseases. *Oxid. Med. Cell. Longev.* **2022**, *2022*, 9744771. [PubMed]
41. Engel, M.; Eggert, C.; Kaplick, P.M.; Eder, M.; Röh, S.; Tietze, L.; Namendorf, C.; Arloth, J.; Weber, P.; Rex-Haffner, M.; et al. The Role of m(6)A/m-RNA Methylation in Stress Response Regulation. *Neuron* **2018**, *99*, 389–403.e9. [CrossRef] [PubMed]
42. Winkler, R.; Gillis, E.; Lasman, L.; Safra, M.; Geula, S.; Soyris, C.; Nachshon, A.; Tai-Schmiedel, J.; Friedman, N.; Le-Trilling, V.T.K.; et al. m^6A modification controls the innate immune response to infection by targeting type I interferons. *Nat. Immunol.* **2019**, *20*, 173–182. [CrossRef] [PubMed]

43. Bechara, R.; Amatya, N.; Bailey, R.D.; Li, Y.; Aggor, F.E.Y.; Li, D.D.; Jawale, C.V.; Coleman, B.M.; Dai, N.; Gokhale, N.S.; et al. The m^6A reader IMP2 directs autoimmune inflammation through an *IL-17*- and *TNFα*-dependent C/EBP transcription factor axis. *Sci. Immunol.* **2021**, *6*, eabd1287. [CrossRef] [PubMed]
44. Zhou, X.; Shen, X. Cecropin supplementation improves growth performance by regulating immune function, rumen fermentation and microbiota in goats. *Anim. Biosci.* **2025**, *38*, 2651–2664. [CrossRef] [PubMed]
45. Zhou, X.; Khan, A.; Xiang, W.; Shen, X. Integrated multi-omics reveals Enterococcus faecalis JM263 alleviates high-concentrate diet-induced hepatic injury via the gut-liver axis in goats. *Microbiome* **2026**, *14*, 178. [CrossRef] [PubMed]

Disclaimer/Publisher's Note: The statements, opinions and data contained in all publications are solely those of the individual author(s) and contributor(s) and not of MDPI and/or the editor(s). MDPI and/or the editor(s) disclaim responsibility for any injury to people or property resulting from any ideas, methods, instructions or products referred to in the content.